

## Article

# Geochemical Characterization of the Eocene Coal-Bearing Source Rocks, Xihu Sag, East China Sea Shelf Basin, China: Implications for Origin and Depositional Environment of Organic Matter and Hydrocarbon Potential

Xiong Cheng <sup>1,2,\*</sup> , Dujie Hou <sup>1,2,\*</sup>, Xinhui Zhou <sup>3</sup>, Jinshui Liu <sup>4</sup>, Hui Diao <sup>4</sup> and Lin Wei <sup>1,2</sup>

<sup>1</sup> School of Energy Resources, China University of Geosciences, Beijing 100083, China; wei.sherry1989@gmail.com

<sup>2</sup> Key Laboratory of Marine Reservoir Evolution and Hydrocarbon Accumulation Mechanism, Ministry of Education, Beijing 100083, China

<sup>3</sup> Hainan Branch of China National Offshore Oil Corporation, Haikou 570100, China; zhouxh3@cnoc.com.cn

<sup>4</sup> Shanghai Branch of China National Offshore Oil Corporation, Shanghai 200050, China; liujsh3@cnoc.com.cn (J.L.); diaohui@cnoc.com.cn (H.D.)

\* Correspondence: xcheng2015@cugb.edu.cn (X.C.); hdj@cugb.edu.cn (D.H.)



check for updates

**Citation:** Cheng, X.; Hou, D.; Zhou, X.; Liu, J.; Diao, H.; Wei, L.

Geochemical Characterization of the Eocene Coal-Bearing Source Rocks, Xihu Sag, East China Sea Shelf Basin, China: Implications for Origin and Depositional Environment of Organic Matter and Hydrocarbon Potential.

*Minerals* **2021**, *11*, 909. <https://doi.org/10.3390/min11080909>

Academic Editors:

Armelle Riboulleau and  
Suryendu Dutta

Received: 29 July 2021

Accepted: 20 August 2021

Published: 23 August 2021

**Publisher's Note:** MDPI stays neutral with regard to jurisdictional claims in published maps and institutional affiliations.

**Abstract:** Eocene coal-bearing source rocks of the Pinghu Formation from the W-3 well in the western margin of the Xihu Sag, East China Sea Shelf Basin were analyzed using Rock-Eval pyrolysis and gas chromatography–mass spectrometry to investigate the samples' source of organic matter, depositional environment, thermal maturity, and hydrocarbon generative potential. The distribution patterns of n-alkanes, isoprenoids and steranes, high Pr/Ph ratios, abundant diterpanes, and the presence of non-hopanoid triterpanes indicate predominant source input from higher land plants. The contribution of aquatic organic matter was occasionally slightly elevated probably due to a raised water table. High hopane/sterane ratios and the occurrence of bicyclic sesquiterpanes and A-ring degraded triterpanes suggest microbial activity and the input of microbial organisms. Overwhelming predominance of gymnosperm-derived diterpanes over angiosperm-derived triterpanes suggest a domination of gymnosperms over angiosperms in local palaeovegetation during the period of deposition. The high Pr/Ph ratios, the plot of Pr/n-C<sub>17</sub> versus Ph/n-C<sub>18</sub>, the almost complete absence of gammacerane, and the distribution pattern of hopanes suggest that the samples were deposited in a relatively oxic environment. Generally, fluctuation of redox potential is coupled with source input, i.e., less oxic conditions were associated with more aquatic organic matter, suggesting an occasionally raised water table. Comprehensive maturity evaluation based on Ro, T<sub>max</sub>, and biomarker parameters shows that the samples constitute a natural maturation profile ranging from marginally mature to a near peak oil window. Hydrogen index and atomic H/C and O/C ratios of kerogens suggest that the samples mainly contain type II/III organic matter and could generate mixed oil and gas.

**Keywords:** biomarkers; higher plant; organic matter; palaeoenvironment; thermal maturity; petroleum potential



**Copyright:** © 2021 by the authors. Licensee MDPI, Basel, Switzerland. This article is an open access article distributed under the terms and conditions of the Creative Commons Attribution (CC BY) license (<https://creativecommons.org/licenses/by/4.0/>).

## 1. Introduction

Source rocks are capable of generating petroleum [1]. Coal and coal measure mudstone are organically rich and generally considered as gas-prone source rock, with some exceptions [2–5]. The formation and distribution of source rocks is mainly controlled by sedimentary basin, palaeoclimate, palaeohydrodynamic conditions, productivity, and preservation of organic matter [6]. Therefore, geochemical characterization of the source rocks is a key to understanding their type and origin of organic matter, thermal maturity, capacity for hydrocarbon generation, palaeoceanographic, and paleoclimatic conditions [7,8].

The Xihu Sag is the most petroliferous region within the East China Sea Shelf Basin (ECSSB), China. The coal-bearing Pinghu Formation ( $E_2p$ ) of middle–late Eocene has been regarded as the primary source rock unit in the Xihu Sag. The  $E_2p$  is organically rich, with large thickness, extensive distribution, and a proper thermal maturity [9,10]. Additionally, oil/gas-source rock correlations support the  $E_2p$  as the primary source rock in the Xihu sag [11–13]. Thus far, a limited number of studies on biomarkers in the  $E_2p$  source rocks have been documented. For instance, Fu [14] reported the occurrence of diterpenoids in coal measures. Zhu et al. [11] systematically studied molecular composition of Paleogene coal-bearing source rocks and discussed their significance for source input. Zhu et al. [9] documented the hydrocarbon potential of Paleogene source rocks, in which distributions of n-alkanes, steranes, and hopanes were simply discussed for investigating the origin of organic matter, depositional environment, and thermal maturity. They found that the source rocks are dominated by Type III-II<sub>2</sub> kerogens (HI = 41–386 mg HC/g TOC) within sub-oxic to oxic environments (Pr/Ph = 1.08–9.78). However, C<sub>29</sub> diasteranes in some samples were incorrectly attributed to C<sub>27</sub> regular steranes by Zhu et al. [9]; therefore, the interpretation based on sterane distributions could be problematic. Cheng et al. [15] compared the geochemical characteristics between a coal and mudstone from the  $E_2p$  and found that they contain predominantly terrigenous source materials with the effect of microbial reworking and were deposited under oxic conditions within an unstratified water column; the mudstone has slightly more algal material input and less oxic conditions during deposition than the coal. Kang et al. [16] studied the organic geochemical and petrological characteristics of the coals of the  $E_2p$ . They found that the coals were deposited under relatively oxic peatland conditions (Pr/Ph = 3.33–9.23) with a predominance of terrestrial higher plants input and have entered the hydrocarbon generation threshold. However, a detailed biomarker study on the  $E_2p$  source rocks for elucidating the organic matter source and depositional characteristics changes over time is lacking in the Xihu Sag.

In 2019, a petroleum exploration well (W-3) located in the Pinghu Slope, western margin of the Xihu Sag (Figure 1), penetrated the  $E_2p$ , and many sidewall cores and a 15.1 m core, including an organic-rich mudstone/carbonaceous mudstone interval, were obtained. This provided a rare opportunity to investigate detailed biomarker distributions of the  $E_2p$  to elucidate the successive changes in source input and depositional environment over time. In this study, the bulk geochemical characteristics and aliphatic hydrocarbon composition of 16 source rocks of the  $E_2p$  were characterized to enhance understanding of the origin of organic matter, depositional environment, thermal maturity, and hydrocarbon generation potential. The results of this study could be beneficial for better understanding the formation mechanism and heterogeneity of the coal-bearing source rocks, which will provide guidance for predicting the formation and distribution of high-quality source rocks. In addition, they could be useful for any oil–oil and oil–source correlations stemming from future exploration in the Xihu Sag.

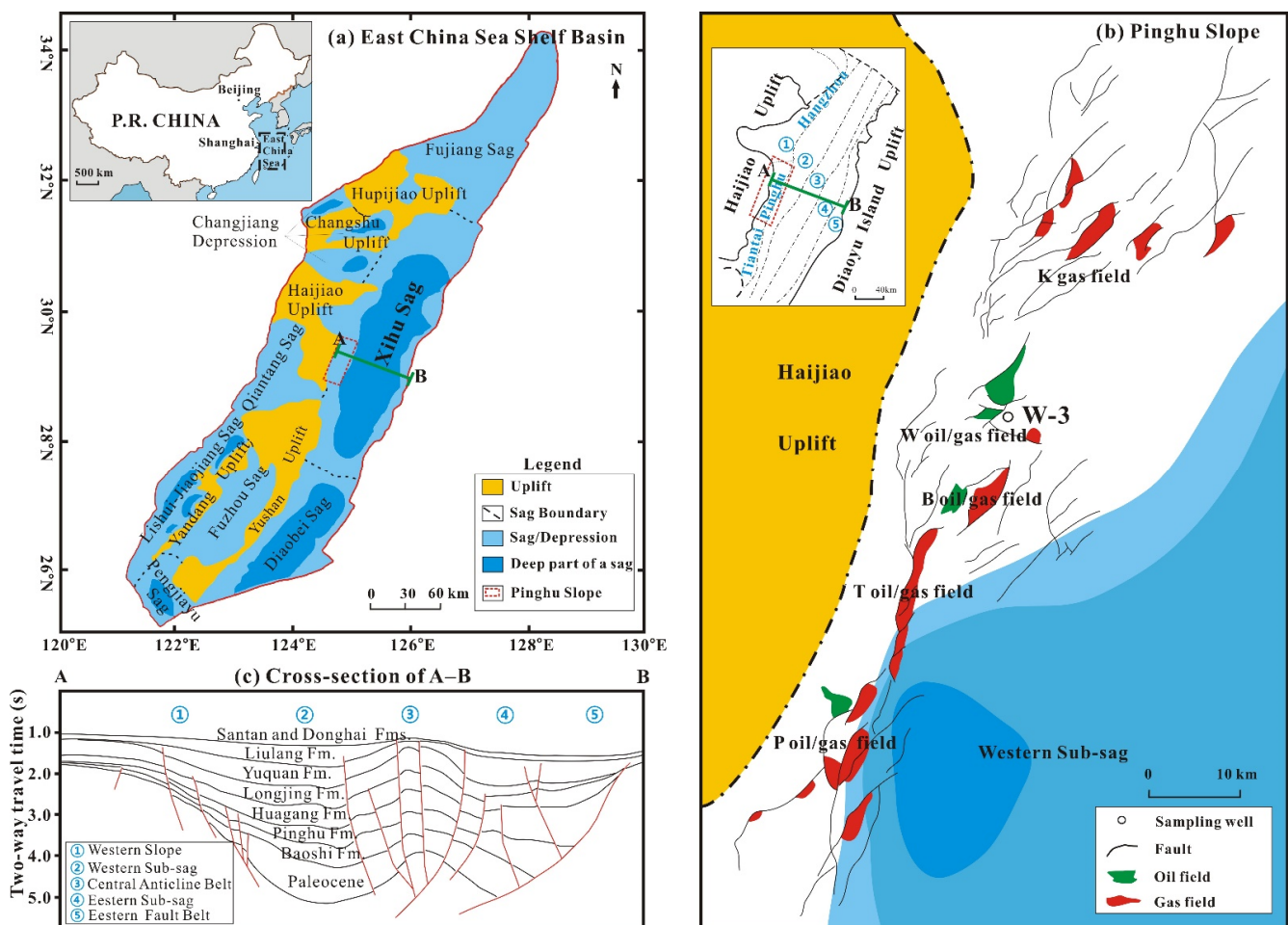


**Figure 1.** Map showing (a) tectonic sketch of the East China Sea Shelf Basin (ECSSB), (b) Pinghu Slope of the Xihu Sag, ECSSB, and (c) structural cross-section of the Xihu Sag (A–B, shown in Figure 1a,b). (adapted from [17]).

## 2. Geological Setting

The Cenozoic ECSSB is located off of the southeast coast of mainland China to the west of the Ryukyu Islands (Japan) [18] (Figure 1a). It is NNE–SSW trending and covers an area of 240,000 km<sup>2</sup>. The Xihu Sag is in the central east of the ECSSB with an area of 46,000 km<sup>2</sup>. The Xihu Sag involves five structural units of which the Western Slope, from north to south, can be further divided into the Hangzhou, Pinghu, and Tiantai slopes (Figure 1b,c). The Xihu Sag is the most petroleum-rich region in the ECSSB, where seven gas/condensate fields and 11 petroleum-bearing structures have been discovered with proved natural gas reserves of  $103.3 \times 10^9$  m<sup>3</sup>, and the Pinghu Slope is the most petroliferous area in the Xihu Sag where a suite of oil and gas fields have been discovered (Figure 1b) [10].

The tectonic evolution of the Xihu Sag includes three main stages: (1) rifting stage during the Paleocene to late Eocene, (2) post-rift stage during late Eocene to late Miocene, and (3) regional subsidence stage since the end of Miocene [19]. The Xihu Sag was filled with Paleogene–Quaternary succession up to 10,000 m (Figure 2a). Of these strata, the E<sub>2p</sub> has a thickness of 600–5000 m, and consists of mudstones, carbonaceous mudstones, coal seams, siltstones, and sandstones (Figure 2b) deposited in tidal delta and tidal flat facies [20]. Seismic sequence and the archive of marine palaeontological fossil suggest that there were frequent transgressions and regressions during the deposition of the E<sub>2p</sub> [21], and the fluctuating water levels and intermittent flooding during the deposition of peat resulted in the interbedded coal, mudstone, and sandstone [22]. The mudstones, carbonaceous mudstones, and coals have been recognized as the major source rocks in the Xihu Sag [11–13], and the accumulative thickness of the coal measuring mudstones is up to

2500 m with an average value of >1000 m and the coals are up to 65 m in the E<sub>2</sub>p [23,24]. The siltstones and sandstones are the major reservoir intervals and the mudstones in the Pinghu and Huagang formations constitute the seal.

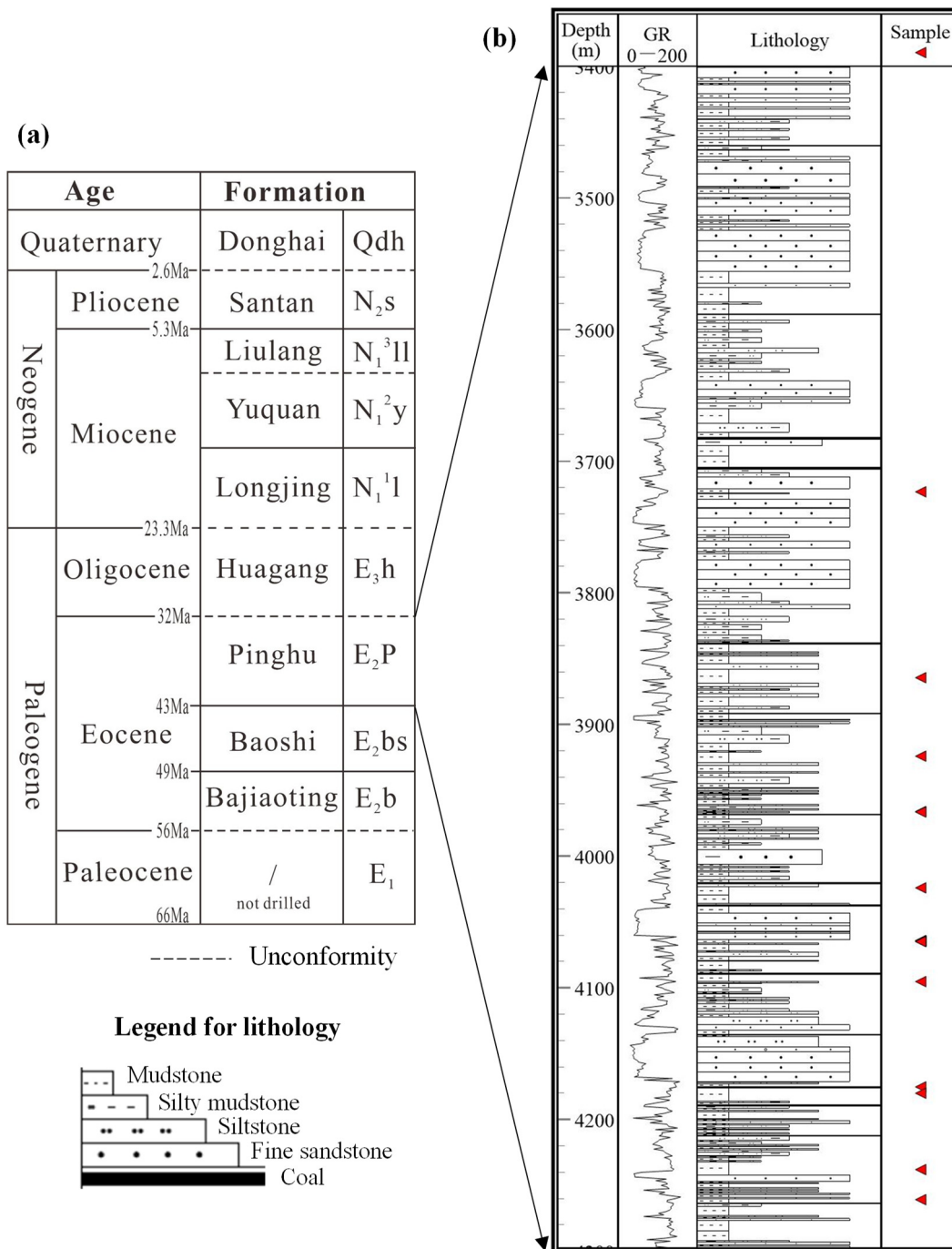


**Figure 2.** A generalized stratigraphy of the Xihu Sag (a) and stratigraphic column showing lithology of the middle–upper Eocene Pinghu Formation from well W-3 and sample locations (b).

### 3. Materials and Methods

#### 3.1. Samples

In this study, a total of 16 samples, including 11 sidewall cores and five cores, of the E<sub>2</sub>p (Figure 2b) were collected from the W-3 well situated in the Pinghu Slope of the Xihu Sag. The W-3 well was drilled with water and no oil-based mud was used. The sidewall

cores were selected from a set of sidewall cores obtained during drilling based on their lithology. The rest five cores were collected from the dark color mudstone interval of the 4050.00–4067.95 m core (15.1 m recovered) continuous core. The samples consist of 12 mudstones, three carbonaceous mudstones, and one coal. The location of the well is shown in Figure 1b, and the origin of the samples is presented in Table 1. The samples were washed with deionized water, and then cleaned with a 9:1 dichloromethane methanol mixture before pretreatment for further analysis.

**Table 1.** Origin and bulk properties of the Eocene Pinghu Formation source rock samples from well W-3, Xihu Sag.

Depth (m)	Sample Type	Lithology	TOC (%)	T <sub>max</sub> (°C)	S <sub>1</sub> (mg/g)	S <sub>2</sub> (mg/g)	S <sub>1</sub> + S <sub>2</sub> (mg/g)	HI (mg/g)	Atomic H/C	Atomic O/C	Ro (%)
3723	Sidewall core	Mudstone	0.81	436	0.15	0.75	0.90	93	nd	nd	0.57
3864.5	Sidewall core	Mudstone	0.29	435	0.19	0.41	0.60	141	nd	nd	0.58
3924	Sidewall core	Mudstone	1.90	440	0.66	2.45	3.11	129	0.84	0.10	0.58
3966	Sidewall core	Coal	60.28	441	8.36	199.92	208.28	332	0.92	0.11	0.60
3966.5	Sidewall core	Carbonaceous mudstone	9.09	440	4.01	43.51	47.52	479	1.03	0.17	0.58
4024	Sidewall core	Mudstone	0.49	441	0.29	0.47	0.76	96	0.82	0.17	0.64
4063.8	Core	Mudstone	2.82	443	0.61	4.87	5.48	173	0.90	0.13	0.63
4064.3	Core	Carbonaceous mudstone	11.39	444	2.91	30.85	33.76	271	0.90	0.14	0.66
4064.5	Core	Mudstone	1.49	445	0.31	1.79	2.10	120	1.12	0.22	0.67
4064.7	Core	Mudstone	0.84	445	0.22	0.94	1.16	112	nd	nd	0.66
4065	Core	Carbonaceous mudstone	7.41	445	1.84	19.68	21.52	266	0.90	0.11	0.66
4095	Sidewall core	Mudstone	3.29	445	1.36	6.89	8.25	209	0.88	0.10	0.60
4175	Sidewall core	Mudstone	3.40	449	1.45	5.35	6.80	157	0.87	0.10	0.68
4180	Sidewall core	Mudstone	0.96	453	0.57	0.87	1.44	91	0.80	0.14	0.70
4238	Sidewall core	Mudstone	0.90	454	0.53	0.93	1.46	103	0.80	0.13	0.74
4260.9	Sidewall core	Mudstone	1.07	454	0.86	1.34	2.20	125	0.80	0.13	0.75

### 3.2. Total Organic Carbon, Rock-Eval Pyrolysis, Vitrinite Reflectance Measurement, and Elemental Composition of Kerogen

The samples were ground (<100 mesh) and homogenized prior to further treatment. The total organic carbon (TOC) contents were determined on samples pretreated with 10 vol% HCl using a LECO CS230 instrument. Source rock pyrolysis was performed using a Rock-Eval instrument following standard methods described by Peters [25]. Briefly, ground whole rock samples weighing up to about 100 mg are pyrolyzed at 300 °C for 3 min (yielding S<sub>1</sub> peak), followed by programmed pyrolysis at 25 °C/min to 600 °C (yielding S<sub>2</sub> peak), both in a helium atmosphere. Rock-Eval parameters, i.e., S<sub>1</sub> (free hydrocarbons, mg HC/g rock), S<sub>2</sub> (pyrolysis hydrocarbons, mg HC/g rock), and T<sub>max</sub> (temperature of maximum pyrolysis yield during the formation of S<sub>2</sub> peak, °C) were determined, and the hydrogen index (HI = S<sub>2</sub>/TOC × 100, mg HC/g TOC) was calculated from the pyrolysis data and the TOC values (Table 1). Both TOC content and Rock-Eval pyrolysis were analyzed at the Experimental Center of China National Offshore Oil Corporation, Shanghai, China (ECCNOOC).

Mean random vitrinite reflectance (Ro) measurements were performed on the surface of vitrinite particles under oil immersion on a TIDAS S MSP400 microscope spectrometer and using standard procedures also at ECCNOOC.

Kerogens were isolated from the powdered samples using HCl/HF digestion. The elemental composition of kerogen (C, H, O and N) was measured using Elementar Vario Cube at China University of Petroleum, Beijing.

### 3.3. Solvent Extraction, Fractionation, and Gas Chromatography–Mass Spectrometry (GC–MS)

The rock powders were Soxhlet-extracted with chloroform for 72 h and then aliquots of the extractable organic matter (EOM) were separated into asphaltenes, saturates, aromatics, and polar compounds using column chromatography [26].

The saturated hydrocarbons were analyzed using a Thermo Trace DSQ II GC–MS at ECCNOOC. An HP-5ms GC column (30 m × 0.25 mm × 0.25 μm) was used to separate the hydrocarbons. The oven temperature was programmed as follows: 50 °C for 1 min, 50–120 °C at a rate of 20 °C/min, 120–250 °C at 3 °C/min, and 250–320 °C at 2 °C/min with a final hold of 20 min. The electron ionization source was operated at 70 eV. Helium was used as carrier gas at a flow rate of 1.0 mL/min. The MS was operated in selected ion monitoring mode. Identification of individual compounds was based on elution order and published mass spectra [17,27,28]. Biomarker parameters were calculated from peak areas integrated in the mass chromatograms using Chemstation.

## 4. Results

### 4.1. Bulk Geochemical Parameters

The bulk geochemical properties of the studied samples are presented in Table 1. The TOC values for the mudstones and carbonaceous mudstones range between 0.3 and 11.4 wt.% and the TOC content of the coal is 60.3 wt.%. The  $S_1 + S_2$  and HI values of the samples vary between 0.6–208.3 mg HC/g rock and 91–479 mg HC/g TOC, respectively. The  $T_{max}$  values range between 435 and 454 °C. The atomic H/C and O/C ratios for the kerogens are in the ranges of 0.80–1.12 and 0.10–0.22. The cross-plots of  $S_2$  versus TOC, HI versus  $T_{max}$  and atomic H/C versus O/C are shown in Figure 3. Vitrinite reflectance (Ro) of the analyzed samples varies between 0.53% and 0.76% (Table 1). Ro and  $T_{max}$  both increase gradually downwards (Figure 4a,b).

### 4.2. Molecular Composition of Aliphatic Hydrocarbons

The molecular composition, derived from GC-MS of the aliphatic fractions, provides valuable information for origin, depositional environment, and thermal maturity of organic matter preserved in the source rocks.

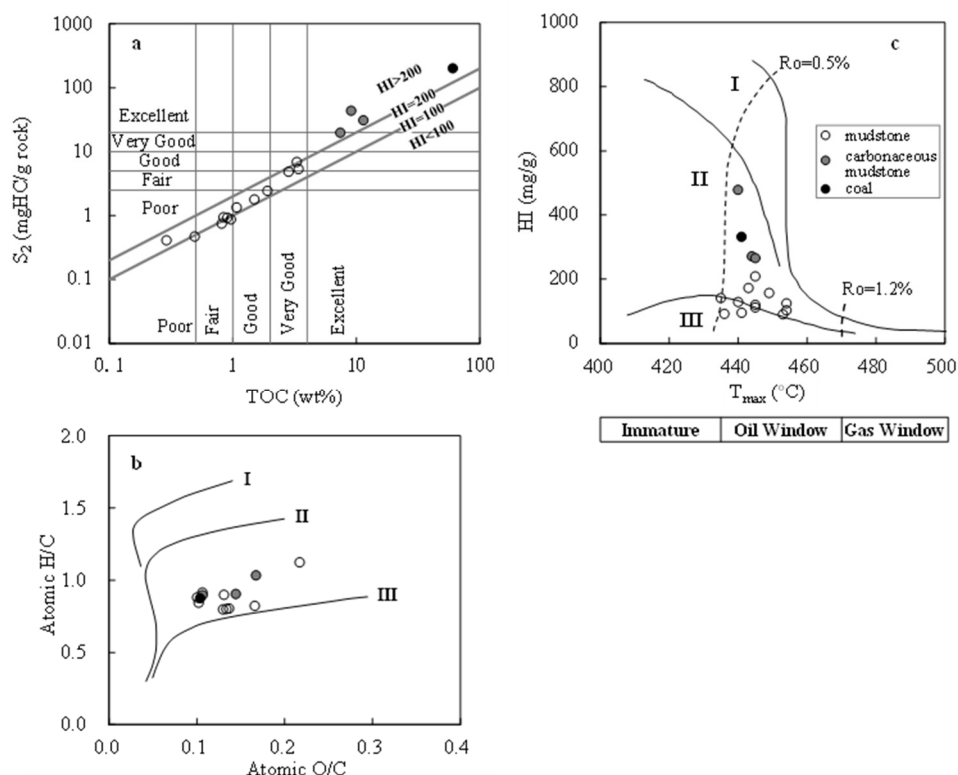


**Figure 3.** Cross-plots of  $S_2$  versus TOC (a), atomic H/C versus O/C (b), and HI versus  $T_{max}$  (c) for source rocks of the Pinghu Formation from well W-3, Xihu Sag. See Figure 3c for the legend.

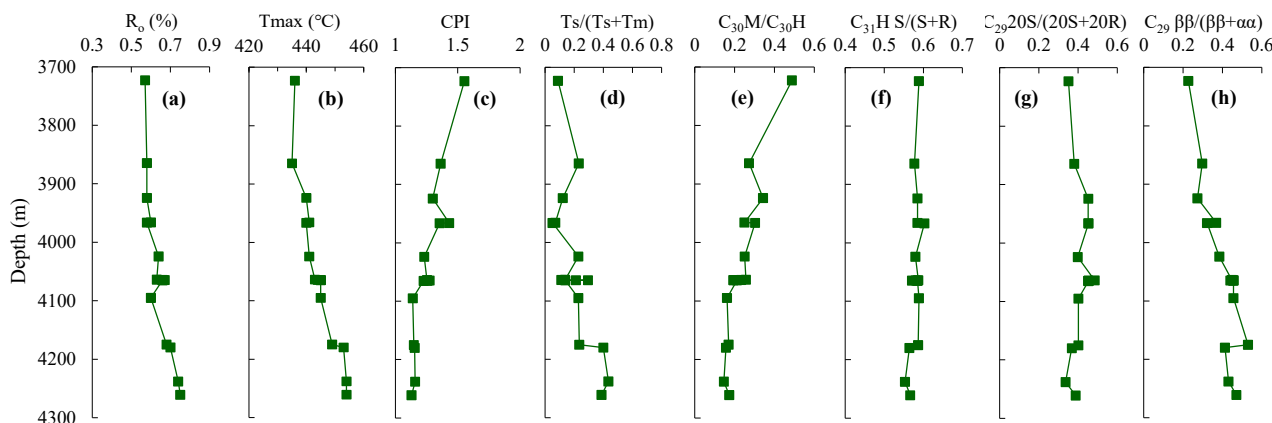


**Figure 4.** Variation of vitrinite reflectance  $R_o$  (a),  $T_{max}$  (b), CPI (c),  $T_s/(T_s + T_m)$  (d),  $C_{30}$  moretane/ $C_{30}$   $\alpha\beta$ -hopane  $C_{30}M/C_{30}H$  (e),  $C_{31}$   $\alpha\beta$ -homohopane  $22S/(22S + 22R)$  (f), and  $C_{29}$  steranes  $\alpha\alpha 20S/(20S + 20R)$  (g) and  $\beta\beta/(\beta\beta + \alpha\alpha)$  (h) with depth for the studied source rocks.

#### 4.2.1. n-Alkanes and Acyclic Isoprenoids

The total ion chromatograms of representative aliphatic fractions and corresponding  $m/z$  85 mass chromatograms are shown in Figure 5. n-Alkanes dominate the aliphatic fractions ranging from  $C_{14}$  to  $C_{35}$ . One exception is the coal at depth of 3966 m in which diterpanes are the dominant components (Figure 5). The n-alkanes are dominated by components of intermediate to long chain lengths with >21 carbon atoms (56–84% of the total n-alkanes); the low-molecular weight n-alkanes ( $n-C_{14}$ – $n-C_{20}$ ) are present in lower proportions (16–44%, mainly <25% of the total n-alkanes; Table 2). The samples from the upper part of the  $E_{2p}$  show evident odd over even n-alkane predominance, which gradually disappear with increasing depth (Figure 5). As a result, the carbon preference index (CPI) [29] decreases with depth (Figure 4c). The commonly used source

indicators, e.g., terrigenous/aquatic ratio (TAR) [30], proxy aqueous ( $P_{aq}$ ) [31] and proxy wax ( $P_{wax}$ ) [32], are highly variable, ranging from 0.73 to 3.89, 0.43 to 0.71 and 0.45 to 0.68, respectively (Figure 6b,c). As expected, TAR positively correlates with  $P_{wax}$ , and TAR and  $P_{wax}$  both negatively correlate with  $P_{aq}$  (Supporting Information Figure S1). CPI, TAR,  $P_{aq}$ , and  $P_{wax}$  are calculated as follows:

$$CPI = 1/2 \times [(n-C_{25} + n-C_{27} + n-C_{29} + n-C_{31} + n-C_{33}) / (nC_{26} + nC_{28} + nC_{30} + n-C_{32} + n-C_{34}) + (n-C_{25} + n-C_{27} + n-C_{29} + n-C_{31} + n-C_{33}) / (n-C_{24} + nC_{26} + nC_{28} + nC_{30} + nC_{32})]$$

$$TAR = (n-C_{27} + n-C_{29} + n-C_{31}) / (n-C_{15} + n-C_{17} + n-C_{19})$$

$$P_{aq} = (n-C_{23} + n-C_{25}) / (n-C_{23} + n-C_{25} + n-C_{29} + n-C_{31})$$

$$P_{wax} = (n-C_{27} + n-C_{29} + n-C_{31}) / (n-C_{23} + n-C_{25} + n-C_{27} + n-C_{29} + n-C_{31})$$

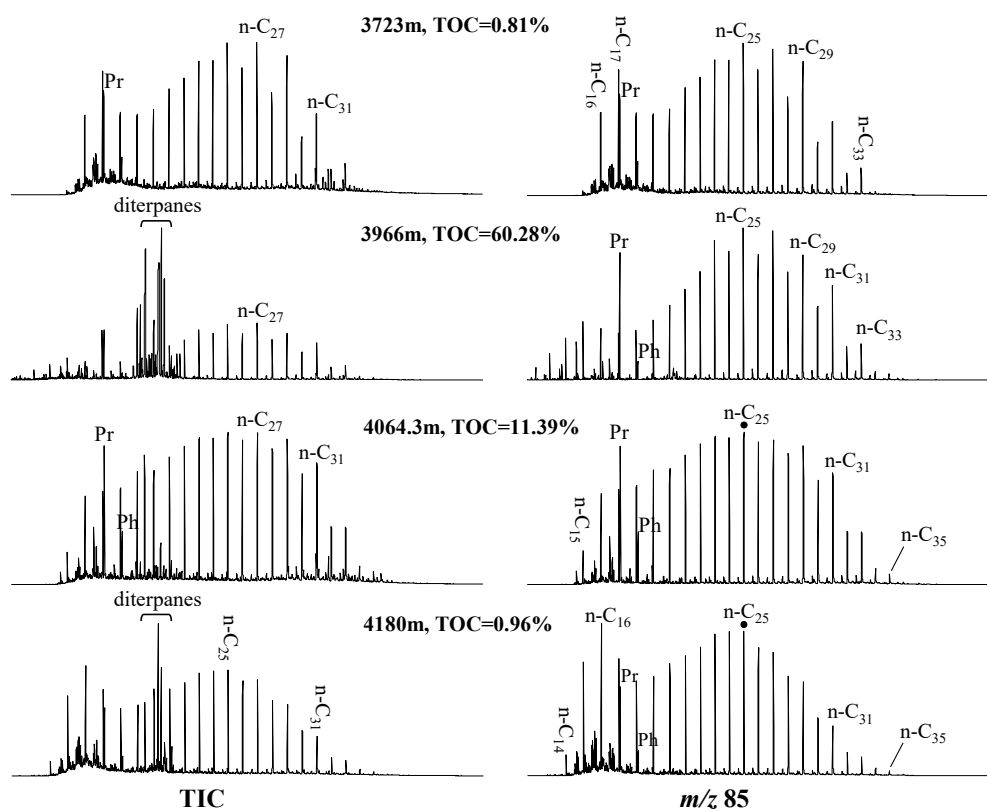


**Figure 5.** Total ion chromatograms and  $m/z$  85 mass chromatograms of aliphatic fractions of the samples. The prominent peaks eluting between  $n-C_{19}$  and  $n-C_{21}$  have been identified as tri- and tetracyclic diterpanes derived from conifer resins.

**Table 2.** Partial source related parameters of the studied source rock samples from the Xihu Sag.

Depth (m)	n-C <sub>14–20</sub> / n-alkanes	n-C <sub>21–25</sub> / n-alkanes	n-C <sub>26–35</sub> / n-alkanes	C <sub>24</sub> TeT/ C <sub>26</sub> TT	C <sub>27</sub> (%)	C <sub>28</sub> (%)	C <sub>29</sub> (%)	C <sub>27</sub> (%)	C <sub>27</sub> /C <sub>29</sub> ααα20R
3723	0.21	0.33	0.46	1.56	14	19	67	14	0.21
3864.5	0.44	0.27	0.29	1.09	16	23	61	16	0.27
3924	0.16	0.28	0.56	2.24	12	17	71	12	0.17
3966	0.16	0.32	0.51	4.27	7	17	76	7	0.10
3966.5	0.21	0.39	0.40	6.19	9	16	75	9	0.12
4024	0.36	0.30	0.34	1.38	26	27	47	26	0.56
4063.8	0.18	0.33	0.49	1.78	7	18	74	7	0.10
4064.3	0.19	0.30	0.51	3.10	7	16	76	7	0.10
4064.5	0.17	0.33	0.50	1.23	13	19	68	13	0.19
4064.7	0.19	0.31	0.50	1.20	18	21	61	18	0.29
4065	0.18	0.28	0.53	5.44	11	19	71	11	0.15
4095	0.24	0.30	0.46	17.26	13	22	66	13	0.19
4175	0.24	0.34	0.41	7.73	14	21	65	14	0.22
4180	0.31	0.33	0.36	1.85	24	27	49	24	0.50
4238	0.29	0.36	0.35	2.04	22	26	51	22	0.43
4260.9	0.36	0.36	0.29	2.98	19	26	55	19	0.36

C<sub>24</sub>TeT/C<sub>26</sub>TT:  $1/2 \times [(C_{24} \text{ TeT} + C_{26} \text{ TT}) - C_{26} \text{ TT}] / C_{26} \text{ TT}$  (see Figure 9a); O/C<sub>30</sub>H: oleanane/C<sub>30</sub> αβ-hopane; Di/(Di + Tri): diterpanes/(diterpanes + non-hopanoid triterpanes); C<sub>27</sub> (%): the relative percentage of C<sub>27</sub> ααα20R sterane over the total of C<sub>27</sub> to C<sub>29</sub> ααα20R steranes; C<sub>27</sub>/C<sub>29</sub> ααα20R: C<sub>27</sub> ααα20R/C<sub>29</sub> ααα20R sterane.

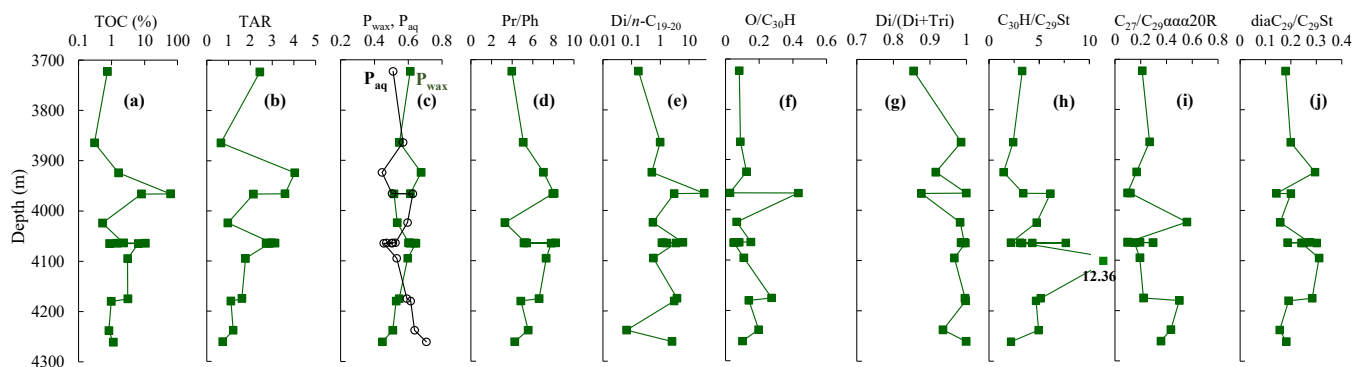


**Figure 6.** Variation of TOC (a), TAR (b), P<sub>aq</sub> (c), P<sub>wax</sub> (c), Pr/Ph (d), diterpanes/*n*-C<sub>19–20</sub> Di/*n*-C<sub>19–20</sub> (e), oleanane/C<sub>30</sub> hopane O/C<sub>30</sub>H (f), diterpanes/(diterpanes + non-hopanoid triterpanes) [Di/(Di + Tri)] (g), C<sub>29</sub> steranes/C<sub>30</sub> hopane C<sub>29</sub>St/C<sub>30</sub>H (h), C<sub>27</sub>/C<sub>29</sub> ααα20R sterane (i), and C<sub>29</sub> diasteranes/C<sub>29</sub> steranes diaC<sub>29</sub>/C<sub>29</sub>St (j) with depth for the studied source rocks.

Acyclic isoprenoids, pristane (Pr), and phytane (Ph), are abundant, especially Pr, which is more prominent than *n*-C<sub>17</sub> in most samples (Figure 5). The Pr/Ph ratios vary between 3.3 and 8.2, and a depth profile of Pr/Ph is presented in Figure 6d. The coaly samples are generally having higher Pr/Ph ratios. The ratios of Pr/*n*-C<sub>17</sub> and Ph/*n*-C<sub>18</sub> range from 0.65 to 7.62 and 0.24 to 0.98, respectively (Figure 7).

#### 4.2.2. Bicyclic to Pentacyclic Terpenoids

Drimane class bicyclic sesquiterpanes with carbon number of C<sub>14</sub>–C<sub>16</sub> were present at extremely low abundance or undetected, and 8β(H)-homodirmane is almost the only visible compound (Supporting Information Figure S2).

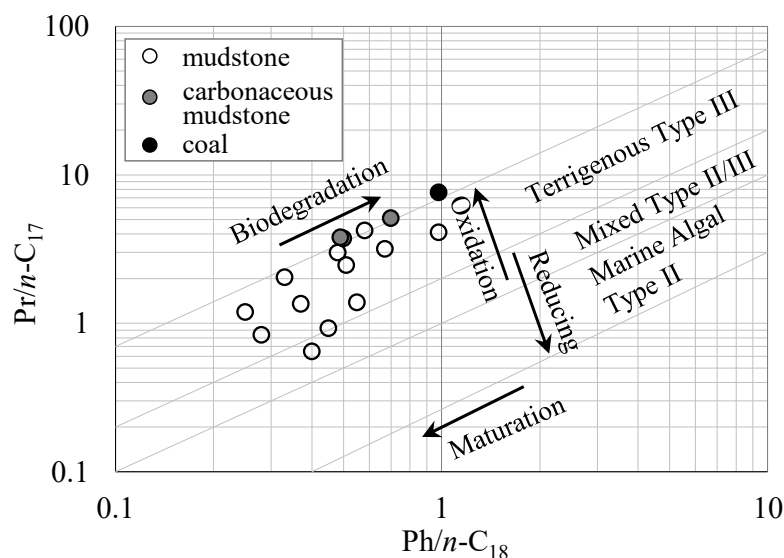


Figure 7. Cross-plot of Pr/n-C<sub>17</sub> versus Ph/n-C<sub>18</sub> for the source rocks of the Pinghu Formation.

Diterpanes, including bi-, tri-, and tetracyclic components, were detected in all samples analyzed (*m/z* 123). They include 8β(H)-labdane (βL), 4β(H)-19-norisopimarane (NIP), fichtelite (18-norabietane, NA), rimuane (R), 17-nortetracyclic diterpane (NT), pimarane (P), ent-beyerane (B), isopimarane (IP), 16β(H)-phyllocladane (βP), abietane (A), and 16α(H)-phyllocladane (αP) (Figure 8). ent-Kauranes (K) were not detected from the samples. The relative abundance of diterpanes varies significantly in the samples (Figure 5). The diterpanes/n-C<sub>19–20</sub> ratios for the mudstones and carbonaceous mudstones are of 0.06–6.10, and the coal has a high ratio of 33.73 (Figure 6e).

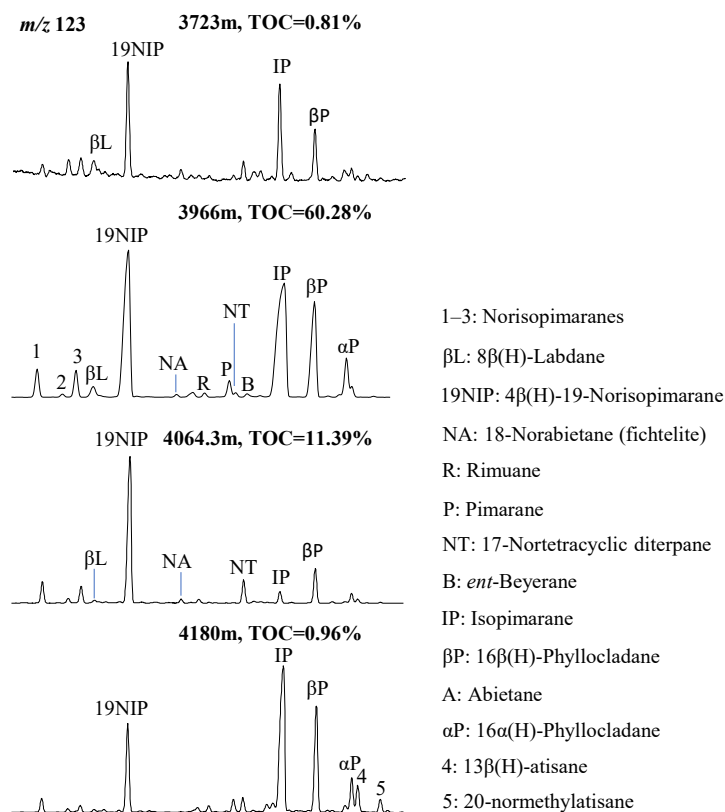
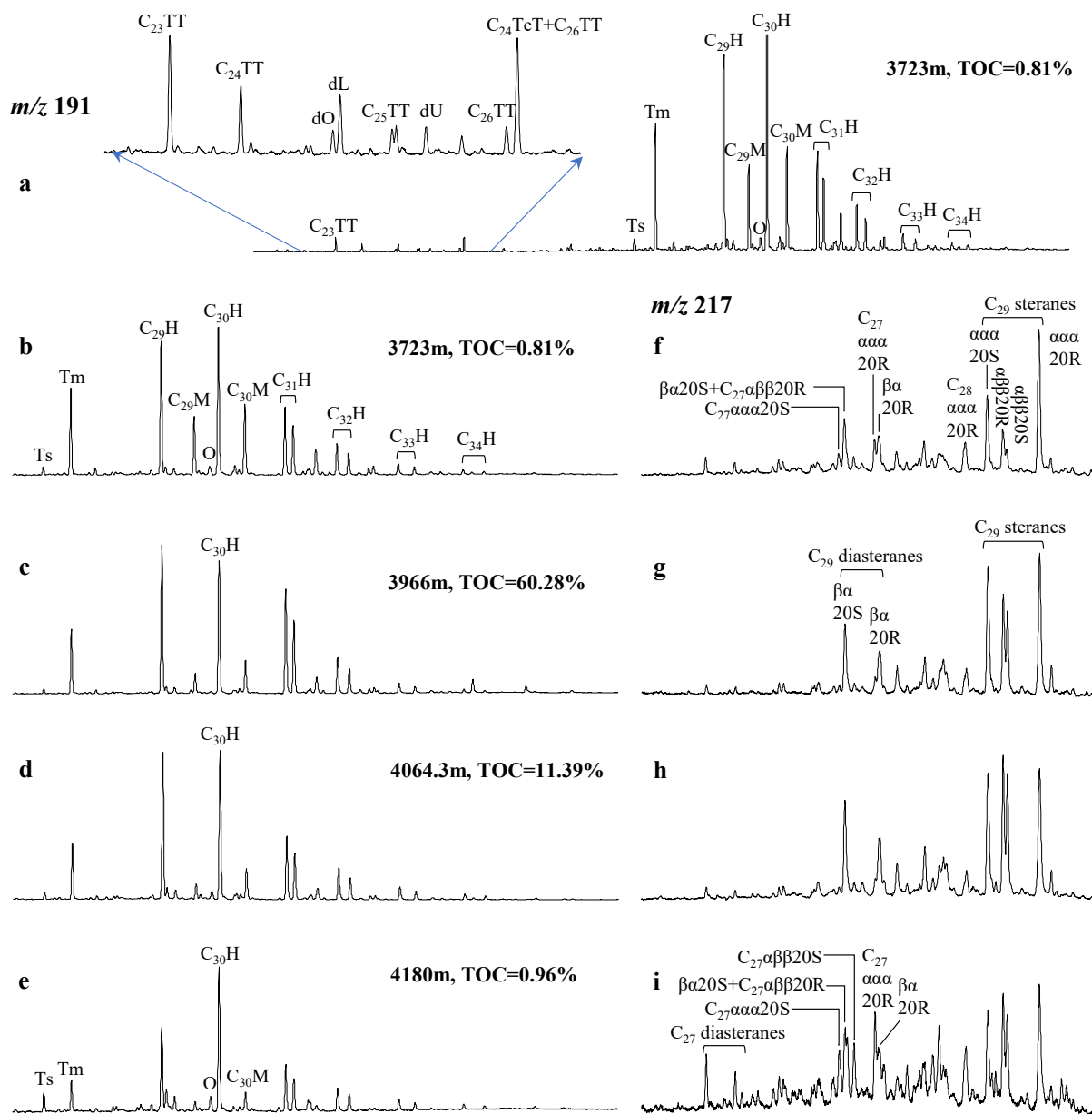


Figure 8. Partial *m/z* 123 mass chromatograms showing distribution of diterpanes.

The abundance of tricyclic terpanes (TT) and C<sub>24</sub> tetracyclic terpene (TeT) are much lower relative to hopanes (Figure 9a). The distribution patterns of C<sub>19</sub>–C<sub>26</sub> TT vary between samples, with a dominance of C<sub>19</sub>–C<sub>21</sub> TT (coal and carbonaceous mudstones) or C<sub>23</sub> TT (mudstones). Although the C<sub>24</sub> TeT was co-eluted with the second isomer of C<sub>26</sub> TT, the former is much more abundant than the latter with the calibrated C<sub>24</sub> TeT/C<sub>26</sub> TT ratios of 1.09–17.26 (Table 2).



**Figure 9.** Partial  $m/z$  191 (a–e) and 217 (f–i) mass chromatograms showing the distribution of tricyclic terpanes, pentacyclic triterpanes and steranes. TT: tricyclic terpene; TeT: tetracyclic terpene; dO: 10 $\beta$ (H)-des-A-oleanane, dL: 10 $\beta$ (H)-des-A-lupane, dU: 10 $\beta$ (H)-des-A-ursane; Ts: 18 $\alpha$ (H)-22,29,30-trinorneohopane; Tm: 17 $\alpha$ (H)-22,29,30-trinorhopane; O: oleanane, H:  $\alpha\beta$ -hopane; M: mortane ( $\beta\alpha$ -hopane).

Angiosperm-derived triterpanes and their diagenetic derivatives, including 10 $\beta$ (H)-des-A-oleanane (dO), 10 $\beta$ (H)-des-A-lupane (dL), 10 $\beta$ (H)-des-A-ursane (dU) and oleanane (O), were identified in all samples at low and variable abundance (Figure 9a). The ratio of oleanane/C<sub>30</sub>  $\alpha\beta$ -hopane (O/C<sub>30</sub>H) for the studied samples are of 0.05–0.43 (Figure 6f). Diterpanes predominate over these triterpenoids with the ratio of diterpanes to the sum

of diterpanes plus non-hopanoid triterpanes [diterpanes/(diterpanes + non-hopanoid triterpanes)] [33] ranging from 0.86 to 1.00 (Figure 6g).

Hopanes (H) with carbon numbers of C<sub>27</sub>–C<sub>34</sub> (without C<sub>28</sub>) were detected in the studied samples (Figure 9a–e). Among them, C<sub>29</sub>–C<sub>31</sub> hopanes are generally more abundant than the other homologues, homohopanes decrease exponentially with increasing carbon number, and rearranged hopanes, including 18 $\alpha$ (H)-22,29,30-trinorneohopane (Ts), 18 $\alpha$ (H)-30-norneohopane (C<sub>29</sub>Ts), and 17 $\alpha$ (H)-diahopane, were present at trace amounts, except the three lowermost samples, as partly shown by the *m/z* 191 mass chromatograms (Figure 9e). The 18 $\alpha$ (H)-22,29,30-trinorneohopane/(18 $\alpha$ (H)-22,29,30-trinorneohopane + 17 $\alpha$ (H)-22,29,30-trinorhopane) [Ts/(Ts + Tm)] ratios are of 0.05–0.43, and generally show an increasing trend with depth (Figure 4d). The C<sub>30</sub> moretane/C<sub>30</sub>  $\alpha\beta$ -hopane (C<sub>30</sub>M/C<sub>30</sub>H) ratios (0.14–0.49) decrease with increasing depth (Figure 4e). The C<sub>31</sub> homohopane 22S/(22S + 22R) ratios range from 0.55 to 0.60 for the studied samples (Figure 4f), which are approximately equal to the endpoints (0.57–0.62) [34]. Gammacerane was almost absent in the sample set, and therefore the commonly used gammacerane index was not calculated.

#### 4.2.3. Steroids

Low abundance of steroids was detected in the analyzed samples by *m/z* 217 mass chromatograms (Figure 9f–i). Among the steroids, C<sub>29</sub> regular steranes predominate over C<sub>27</sub> and C<sub>28</sub> homologues, followed by C<sub>29</sub> diasteranes. The relative abundances of the C<sub>27</sub>, C<sub>28</sub> and C<sub>29</sub>  $\alpha\alpha\alpha$ 20R steranes in the samples are 7–26%, 16–27%, and 47–76%, respectively (Table 2). The ratio of C<sub>30</sub>  $\alpha\beta$ -hopane/C<sub>29</sub> regular steranes (C<sub>30</sub>H/C<sub>29</sub>St) ranges from 1.46 to 12.36, with an average value of 4.46 and is displayed in stratigraphic order shown in Figure 6h. The C<sub>27</sub>/C<sub>29</sub>  $\alpha\alpha\alpha$ 20R sterane ratios of the studied samples vary from 0.10 to 0.56 (Table 2; Figure 6i), and the samples with high ratios are characterized by low TOC values. The C<sub>29</sub> steranes isomerization ratios,  $\alpha\alpha\alpha$ 20S/(20S + 20R) and  $\beta\beta$ /( $\beta\beta$  +  $\alpha\alpha$ ), for the samples range from 0.34 to 0.45 and 0.23 to 0.53, respectively (Table 2), having not reached equilibrium values. Interestingly, the  $\alpha\alpha\alpha$ 20S/(20S + 20R) ratios are relatively stable throughout the profile, except the initial increase with depth (<4000 m) (Figure 4g). In contrast, the C<sub>29</sub> sterane  $\beta\beta$ /( $\beta\beta$  +  $\alpha\alpha$ ) ratios gradually increase downwards, except a negative shift of the three lowermost samples (Figure 4h). The ratio of C<sub>29</sub> diasteranes/C<sub>29</sub> steranes (diaC<sub>29</sub>/C<sub>29</sub>St; peak areas integrated on *m/z* 259 and 217 mass chromatograms, respectively) ranges from 0.14 to 0.31 and shows no regular correlation with depth (Figure 6j).

## 5. Discussion

### 5.1. Source of Organic Matter

#### 5.1.1. Algae, Microorganisms, and Unspecified Higher Plants

Short-chain n-alkanes (< n-C<sub>20</sub>) predominantly originate from algae and microorganisms [35], mid-chain n-alkanes (n-C<sub>21</sub>–n-C<sub>25</sub>), especially n-C<sub>23</sub> and n-C<sub>25</sub>, are reported to originate from submerged/floating aquatic macrophytes or Sphagnum [31], and long-chain n-alkanes (> n-C<sub>25</sub>) are typically considered to derive from epicuticular waxes of vascular plants [36], although some nonmarine algae (e.g., *Botryococcus braunii*) may also contain high molecular-weight n-alkanes [37]. The studied samples contain high abundance of long-chain (n-C<sub>26–35</sub>: 29–53%) and mid-chain (n-C<sub>21–25</sub>: 27–37%) n-alkanes and low abundance of short-chain homologues (n-C<sub>14–20</sub>: 16–44%) (Table 2). This indicates significant contributions from terrestrial higher plants and aquatic macrophytes/sphagnum and relatively low algal/bacterial sources input but with some variations.

TAR reflects relative input of terrigenous versus aquatic OM and high values are indicative of a higher plant input [30]. The relatively high TAR values (mainly >1.0) of the studied samples are consistent with significant source input from higher plants. However, the TAR values are highly variable (Figure 6b), indicating that input of aquatic OM was variable during deposition of these sediments. The P<sub>aq</sub> reflects the input of the non-emergent aquatic macrophytes relative to emergent and terrestrial plants [31]. For the studied samples, this proxy gives values ranging from 0.43 to 0.71 (Figure 6c),

indicating significant submerged or floating macrophyte-derived source materials input. The  $P_{wax}$  reflects the relative proportion of waxy hydrocarbons derived from emergent macrophytes and terrestrial plants [32]. The high  $P_{wax}$  ratios (0.45–0.68) for the samples indicate prominent higher plant input in relation to bulk plant input at low water level. The good correlation among  $P_{aq}$ ,  $P_{wax}$  and TAR (Supporting Information Figure S1) suggest changes in source contribution of aquatic versus terrestrial plants-derived OM through time. CPI was affected by thermal maturation (see Section 5.3) and, therefore, is not reliable for interpreting source contribution. It is worth noting that thermal maturation favors the transformation of high molecular-weight n-alkanes to lower molecular-weight counterparts. Thus, the contributions from algae and microorganisms in the samples from the lower part of the profile would be slightly overestimated.

In the Pr/n-C<sub>17</sub> versus Ph/n-C<sub>18</sub> plot (Figure 7), all the studied samples are plotted in the terrigenous Type III zone, suggesting a dominance of terrigenous OM deposited in oxidizing environments with some fluctuation. This is consistent with the high Pr/Ph ratios. Furthermore, the occurrence of only trace amounts of tricyclic terpanes with high C<sub>24</sub>TeT/C<sub>26</sub>TT ratios also support a terrigenous source of OM in the samples [38].

C<sub>27</sub> and C<sub>28</sub> steroids are derived from phytoplankton, whereas C<sub>29</sub> homologues are mainly derived from terrestrial plants [39]; in addition, C<sub>29</sub> steranes may also originate from brown and certain green algae [40]. Thus, the relative composition of the regular steranes can be used to illustrate the type of OM contributing to the sediments. In this case, the C<sub>29</sub> steranes are more likely to be derived from higher plants according to the tidal delta and tidal flat facies of the E<sub>2p</sub>, and the predominance of C<sub>29</sub> over C<sub>27</sub> and C<sub>28</sub> steranes in the samples indicates major input of higher plant materials.

There is a marked correlation between the distribution of regular steranes and n-alkanes: the samples containing higher amounts of C<sub>27</sub> steranes are characterized by more abundant low molecular-weight n-alkanes, as evidenced by the negative correlation between C<sub>27</sub>/C<sub>29</sub>  $\alpha\alpha\alpha$ 20R sterane and TAR (Supporting Information Figure S1d). This suggests that steranes and n-alkanes are consistent in source interpretation. The lowermost three samples together with the samples at depth of 4024 m and 3864.5 m consistently contain relatively high concentrations of C<sub>27</sub> regular steranes and low molecular-weight n-alkanes and hence the slightly higher C<sub>27</sub>/C<sub>29</sub>  $\alpha\alpha\alpha$ 20R sterane and  $P_{aq}$  ratios and lower TAR values (Figure 6b,c,i), suggesting that these samples have more contribution from aquatic OM. The increased aquatic OM could be related to the raised water table during deposition.

Additionally, the TOC values of the samples were observed to be positively related to TAR and Pr/Ph, and negatively related to C<sub>27</sub>/C<sub>29</sub>  $\alpha\alpha\alpha$ 20R sterane ratios, respectively (Figure 10), supporting the interpretation of a dominant terrestrial OM input.

Hopanoids are derived from degradation of bacteriohopanepolyols in prokaryotes, and are indicative of bacterial OM input [41]. The hopane/sterane ratio indicates the contribution of prokaryotic versus eukaryotic organisms, and high values are associated with input of terrigenous and/or bacterially reworked OM [1]. The high C<sub>30</sub>H/C<sub>29</sub>St ratios for the samples analyzed suggest a significant contribution of bacterial biomass and/or bacterially reworked terrestrial OM. This is consistent with the oxic conditions of the nearshore coal-bearing transitional and marsh facies which are favorable for an enhanced degree of bacterial activity and which in turn produced relatively high amounts of hopanoid precursors. The presence of bicyclic sesquiterpanes also suggests the contribution of bacterial to the OM [42]. In addition, the occurrence of dO, dL, and dU further proved microbial activity, as degraded triterpenoids are thought to be the products of microbial photomimetic decomposition of pentacyclic triterpenoids [43].

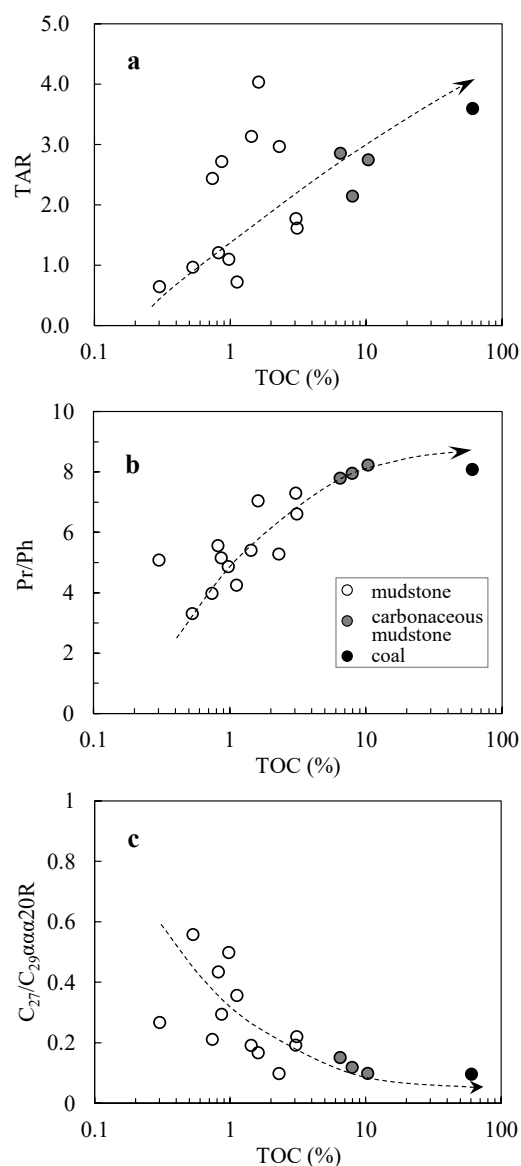


**Figure 10.** Cross-plots of TOC versus TAR (a) Pr/Ph, (b) and C<sub>27</sub>/C<sub>29</sub> ααα20R sterane, (c) for the studied source rocks.

### 5.1.2. Gymnosperm and Angiosperm

Tri- and tetracyclic diterpenoids are derived from conifer (gymnosperm) resins. Diterpenoids with labdane and isopimarane skeleton have been identified in all conifer families except the former family Cephalotaxaceae [44]. Additionally, labdanes could also be originated from microorganisms when accompanied by the C<sub>15</sub>–C<sub>24</sub> homologues [45]. Regular abietane-type diterpenoids are very widespread in conifer families, and they are major components of Pinaceae resins [46,47]. Diterpenoids with phyllocladane structures widely occur in Podocarpaceae, Araucariaceae, Cupressaceae, and Taxodiaceae but are absent in the Pinaceae [44,47]. C<sub>19</sub> diterpanes, e.g., NIPs, NA, and NT, could be derivatives of corresponding C<sub>20</sub> diterpenoid precursors (e.g., conifer resin acids) by decarboxylation and reduction reactions [27,48]. However, NIPs could have additional C<sub>19</sub> precursors present in gymnosperms [49]. Non-hopanoid triterpenoids containing O, L, and U skeletons have long been considered as typical biomarkers for angiosperms [50,51]. They are common constituents of leaf waxes, wood, roots, and bark of angiosperms. Des-A-triterpenoids are probably formed during diagenesis from C<sub>30</sub> precursors [52], although unidentified C<sub>24</sub> precursors could be present [51].

In the studied samples,  $\beta$ L ( $C_{20}$ ) was present but without  $C_{15}$ – $C_{24}$  homologues, indicating a conifer origin of labdane. Therefore, the occurrence of diterpanes with different structural types, distribution patterns, and relative abundance in the analyzed samples reflects varying contributions of various conifer families (Figures 6e and 8). The presence of dO, dL, dU, and O in the studied samples (Figure 9a) ascertains the contribution of angiosperms. However, the taxonomical differentiation between gymnosperm and angiosperm families is not possible based on the molecular composition as they are not species-specific [53,54].

Due to the diagnostic features of diterpanes (conifers) and non-hopanoid triterpanes (angiosperms), the ratio of diterpanes/(diterpanes + non-hopanoid triterpanes) can be used to semi-quantitatively estimate the relative contribution of gymnosperms (specifically conifers) and angiosperms [33]. The abundance of diterpanes relative to n-alkanes show large variations (0.06–33.73), suggesting varying contributions of conifers to the sedimentary OM. However, the diterpanes/(diterpanes + non-hopanoid triterpanes) ratio shows extremely high and uniform values throughout the depth profile (above 0.97, with a few exceptions: 3723 m, 3924 m, 3966.5 m and 4238 m, Figure 6g), indicating an overwhelming predominance of conifers over angiosperms in palaeovegetation. The occasionally lower ratios for the four samples appear to imply variations in compositional changes in the local plant community, where the relative contribution of angiosperms was slightly higher.

In conclusion, the composition of biomarkers in the studied samples suggest predominantly terrigenous organic matter input with subordinate algae and microorganisms. Among the terrigenous organic matter, gymnosperm-derived dominates over angiosperm-derived. Some fluctuations exist as certain intervals contain a greater amount of algae.

## 5.2. Depositional Environment

The Pr/Ph ratio is the most used proxy for redox conditions of water column during deposition [55]. However, it has some limitations due to the influence of additional source materials and thermal maturation [56,57]. Pr/Ph ratio < 0.8 indicates saline to hypersaline conditions and/or reducing conditions, while ratio > 3 reflects terrigenous plant input deposited under oxic to suboxic environments [58]. The high Pr/Ph ratios (3.3–8.2) for the studied samples are indicative of terrigenous OM input under oxic conditions. The vertical variation of Pr/Ph ratios (Figure 6d) indicate periodic changes in redox potential, which might be associated with the fluctuation of the water table during deposition, as consistent with the changes in relative abundance of aquatic OM input. This interpretation further supports the frequent transgression and regression during the deposition of the  $E_{2p}$  as suggested by the seismic sequence and the occurrence of marine palaeontological fossils [21]. The cross-plot of Pr/n- $C_{17}$  versus Ph/n- $C_{18}$  (Figure 7) suggests terrigenous source materials deposited in an oxidizing environmental condition as well. The simple distribution pattern of hopanes characterized by high Tm and  $C_{29}$ – $C_{31}H$  and the exponential decrease of homohopanes without  $C_{35}H$  (Figure 9a–e) are characteristics of hopanoids associated with oxic-type environments [58].

Diasteranes are formed by the rearrangement of steroids during catagenesis by the catalyzation of clay minerals [59]. Highly anoxic environments are favorable for the formation of diasteranes because, within an oxic-type environment, sterenes will be left unreduced and hence available for rearrangement reaction [38,60]. Additionally, high thermal maturity can also result in the enrichment of diasteranes [61]. In this study, the effect of thermal maturity on the dia $C_{29}/C_{29}St$  ratios could be negligible, as the ratio has no positive relationship with thermal maturity/depth (Figure 6j). The mudstones rich in clay have dia $C_{29}/C_{29}St$  ratios of 0.16–0.31 which are not consistently higher than that of the coal and carbonaceous mudstones with low clay and high TOC contents (0.14–0.24, Figure 11a), suggesting that the content of clay minerals does not necessarily exclusively control diasterane formation. Interestingly, there is a positive and negative correlation between the dia $C_{29}/C_{29}St$  and Pr/Ph ratios for the mudstones and coaly samples, respectively (Figure 11b). Therefore, it is possible that oxicity of the depositional environment is a major factor for the enrichment

of diasteranes in the clay samples, while the content of clay minerals controls the formation of diasteranes in coaly samples.

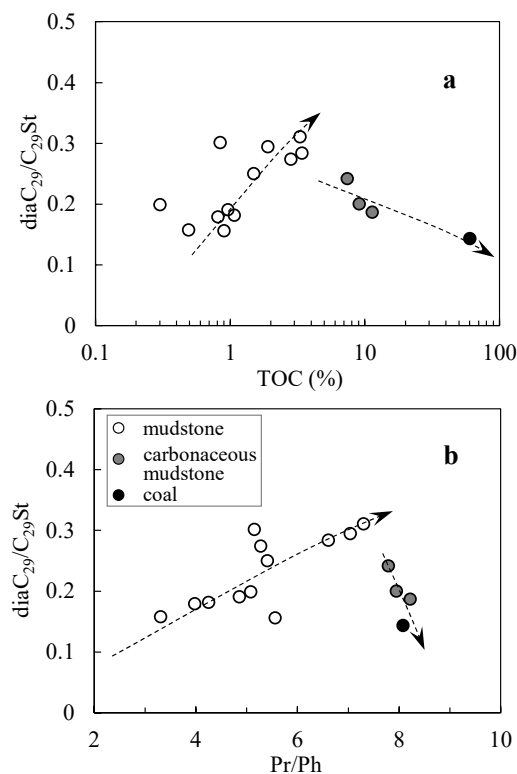


**Figure 11.** Cross-plots of  $C_{29}$  diasteranes/ $C_{29}$  regular steranes ( $\text{dia}C_{29}/C_{29}\text{St}$ ) versus TOC (a) and Pr/Ph (b) for the studied source rocks.

### 5.3. Thermal Maturity

Vitrinite reflectance, Rock–Eval pyrolysis  $T_{\text{max}}$ , and varying biomarker proxies have been widely used to evaluate the thermal maturity of source rocks [58]. A comprehensive thermal maturity evaluation suggests that the studied  $E_{2p}$  samples constitute a natural maturation profile from the marginally mature to mid-mature (onset of oil window to near peak oil window).

The studied samples have  $R_o$  values ranging from 0.53 to 0.76% and therefore are of sub-bituminous A to high volatile bituminous B rank.  $T_{\text{max}}$  values range from 435–454 °C and are thus in agreement with the vitrinite reflectance data [62]. All samples analyzed are therefore in the early mature to mid-mature range.

The CPI, homohopane 22S/(22S+22R), and moretane/hopane ratios are reliable maturity indicators during the immature to low mature stage, decreasing with increasing thermal maturity [29,58]. The moretane/hopane ratios decrease from ~0.8 in immature sediments to <0.15 in mature sediments and petroleum [63]. The  $\alpha\alpha\alpha 20S/(20S + 20R)$  and  $\beta\beta/(\beta\beta + \alpha\alpha)$  ratios based on  $C_{29}$  steranes gradually increase during maturation and meet the endpoints (0.52–0.55 and 0.67–0.71, respectively) at the peak oil window [64]. The  $C_{31}H$  22S/(22S + 22R) ratios for the samples are in equilibrium, suggesting that they have entered the oil window [34]. The elevated CPI and  $C_{30}M/C_{30}H$  values for the upper samples gradually decrease in a downward trend, together with the increasing trend of the  $C_{29}$   $\beta\beta/(\beta\beta + \alpha\alpha)$  steranes ratio without reaching equilibrium points, this all suggesting a natural thermal maturity gradient ranging from marginally mature to the middle oil generation window. This interpretation agrees well with the  $R_o$  values.

The  $T_s/(T_s + T_m)$  ratios broadly increase with depth (Figure 4d), reflecting increasing maturity with depth; however, the significant fluctuation of  $T_s/(T_s + T_m)$  ratios indicate that this parameter could also be affected by other factors, such as lithology (clay minerals) [58]. The relatively constant  $C_{29}$   $\alpha\alpha\alpha 20S/(20S + 20R)$  steranes' ratios throughout

the profile but without reaching the equilibrium values were unexpected. No plausible explanation is available here, but it might be related to the effects of lithofacies and the depositional environment.

#### 5.4. Hydrocarbon Generative Potential and Exploration Implications

The remaining petroleum potential of the Pinghu Formation samples can be characterized using TOC contents and  $S_2$ . TOC and  $S_2$  values for the studied samples are generally greater than 0.5 wt% and 2.0 mg HC/g rock (Table 1), suggesting a range in source rock potential from fair to very good (Figure 3a).

There is now consensus that coal seams and coal-bearing strata can generate liquid hydrocarbons [65]. Oil generation capacity of coaly source rocks depends on hydrogen content in the kerogen, and those hydrogen-rich coaly source rocks are often rich in liptinite (e.g., resinite, sporinite, cutinite) and/or perhydrous vitrinite [65,66]. The source potential of immature kerogens with an HI between 150 and 300 mg/g is generally considered to be gas and oil [67].

The elemental composition of kerogen, the atomic H/C versus O/C diagram, is the most familiar method of classifying kerogen type (Figure 3b) [68]. Rock-Eval derived HI provides a rapid measurement of hydrogen content, and the HI versus  $T_{max}$  cross-plot (Figure 3c) reflects the organic matter type as well. Most of the samples are plotted in the Type II organic matter domain but near the boundary of Type III (Figure 3b,c), suggesting predominantly Type II/III kerogen. The coal and carbonaceous mudstones are characterized by higher HI values (Figure 3a,c), which is commonly observed for coaly samples [69]. The samples with relatively high hydrogen content might be due to high amounts of resinite, as suggested by the abundant diterpanes in the aliphatic fractions (Figure 5) and the maceral composition of other samples taken from this formation [16,23]. The relatively hydrogen-rich nature (Type II/III kerogen) together with maturity at the early to near peak oil window of the samples analyzed suggest that they could be capable of generating some liquid hydrocarbons and significant natural gas at a higher maturity stage [25].

In summary, the composition of biomarkers suggests that the studied samples contain predominantly terrestrial higher plants' (especially gymnosperms rather than angiosperms) derived organic matter with subordinate algae/microorganisms deposited in a relatively oxic, fluvial-deltaic environment. An appropriate water table favorable for peat formation resulted in source rocks with higher TOC and HI values, whereas, during occasional increased water levels, mudstone containing more algae but lower TOC and HI values was developed. These, therefore, suggest that a stable peat environment is the key for high-quality source rock formation in the Xihu Sag. A combination with sedimentologic studies will give further constraints on the distribution of excellent source rocks for petroleum exploration. In addition, not only natural gas but also light oils are worth exploring due to the relatively hydrogen-rich nature of the E<sub>2p</sub> source rocks. However, appropriate thermal maturity is a prerequisite.

## 6. Conclusions

The investigation of the coal-bearing source rocks of the Eocene Pinghu Formation from the W-3 well, western margin of the Xihu Sag, East China Sea Shelf Basin has yielded important new results regarding their organic matter source, depositional environment, thermal maturity, and hydrocarbon generative potential.

Source-related biomarker parameters suggest a dominant contribution from terrigenous higher plant organic matter with subordinate algae/microorganisms in the studied source rock samples. Contributions from aquatic organic matter were increased in certain intervals as suggested by reduced Pr/Ph and TAR and elevated  $P_{aq}$  and  $C_{27}$  steranes, which might indicate the occasional rise of the water table. The occurrence of diterpanes and non-hopanoid triterpanes (oleanane, des-A-oleanane, -ursane, and -lupane) within the source rocks indicates the contribution of conifers (gymnosperms) and angiosperms.

The predominance of gymnosperms in the peat-forming vegetation is evidenced by the dominance of diterpenoids over non-hopanoid triterpanes.

The high Pr/Ph ratios, Pr/n-C<sub>17</sub> versus Ph/n-C<sub>18</sub> cross-plot, dominance of C<sub>29</sub> steranes, distribution of hopanes, and almost complete absence of gammacerane suggest that the source rocks were deposited in relatively oxic environments. Variations in redox potential during deposition were proven by significant fluctuation of Pr/Ph in the profile. Diagenetic rearrangement of steroids to diasteranes could be controlled by both clay minerals and oxicity of the depositional environment.

Vitrinite reflectance, Rock-Eval T<sub>max</sub>, and molecular thermal maturity proxies indicate that the source rock samples constitute a natural maturation profile ranging from a marginally mature to a mid-mature stage.

Kerogen elemental composition and HI values indicate that the source rock samples have Type II/III kerogen, suggesting that they are gas- and oil-prone and are capable of generating oil and gas during thermal maturation. Overall, our results suggest that source rocks with high source potential were formed in a stable peat formation environment. Natural gas and crude oil are worth exploring, which depend on the thermal maturity of the source rock.

**Supplementary Materials:** The following are available online at <https://www.mdpi.com/article/10.3390/min11080909/s1>, Figure S1: Cross-plots of TAR versus Paq (a) and Pwax (b), Paq versus Pwax (c), and TAR versus C<sub>27</sub>/C<sub>29</sub>  $\alpha\alpha\alpha$ 20R sterane (d), Figure S2: Partial *m/z* 123 mass chromatograms showing distribution of bicyclic sesquiterpanes and diterpanes in representative samples.

**Author Contributions:** Conceptualization, X.C. and D.H.; methodology, X.C. and H.D.; software, X.C.; investigation, X.C., D.H., H.D. and L.W.; resources, X.Z., J.L. and H.D.; data curation, X.C. and H.D.; writing—original draft preparation, X.C.; writing—review and editing, X.C. and D.H.; visualization, X.C. and H.D.; supervision, D.H.; project administration, D.H., J.L. and H.D.; funding acquisition, X.C., D.H., J.L., H.D. and L.W. All authors have read and agreed to the published version of the manuscript.

**Funding:** This research was funded by the National Science and Technology Major Project, Grant No. 2016ZX05027-001-003; China Postdoctoral Science Foundation, Grant No. 2019M660735; and Fundamental Research Funds for the Central Universities, Grant No. 26522019013 and 26522018214.

**Institutional Review Board Statement:** Not applicable.

**Informed Consent Statement:** Not applicable.

**Data Availability Statement:** Not applicable.

**Acknowledgments:** The authors acknowledge the three anonymous reviewers for their constructive comments as well as Rita Xu, Assistant Editor, for handling the manuscript.

**Conflicts of Interest:** The authors declare no conflict of interest.

## References

1. Tissot, P.B.; Welte, D.H. *Petroleum Formation and Occurrence*; Springer: Berlin/Heidelberg, Germany, 1984.
2. Difan, H.; Dajiang, Z.; Jinchao, L.; Xiaoming, H. Hydrocarbon genesis of Jurassic coal measures in the Turpan Basin, China. *Org. Geochem.* **1991**, *17*, 827–837. [[CrossRef](#)]
3. Clayton, J.L.; Rice, D.D.; Michael, G.E. Oil-generating coals of the San Juan Basin, New Mexico and Colorado, U.S.A. *Org. Geochem.* **1991**, *17*, 735–742. [[CrossRef](#)]
4. Killops, S.; Woolhouse, A.D.; Weston, R.J.; Cook, R.A. A Geochemical Appraisal of Oil Generation in the Taranaki Basin, New Zealand. *AAPG Bull.* **1994**, *78*, 1560–1585.
5. Petersen, H.I.; Hertle, M. A Review of the Coaly Source Rocks and Generated Petroleum in the Danish North Sea: An Underexplored Middle Jurassic Petroleum System? *J. Pet. Geol.* **2018**, *41*, 135–154. [[CrossRef](#)]
6. Katz, B.J. Controlling Factors on Source Rock Development—A Review of Productivity, Preservation, and Sedimentation Rate. In *The Deposition of Organic-Carbon-Rich Sediments: Models, Mechanisms, and Consequences*; SEPM Society for Sedimentary Geology: Tulsa, OK, USA, 2005; Volume 82, pp. 7–16.
7. Fathy, D.; Wagreich, M.; Ntaflos, T.; Sami, M. Provenance Characterization of Campanian Lacustrine Organic-Rich Mudstones on the Southern Tethyan Margin, Egypt. *ACS Earth Space Chem.* **2021**, *5*, 197–209. [[CrossRef](#)]

8. Fathy, D.; Wagreich, M.; Ntaflos, T.; Sami, M. Paleoclimatic variability in the southern Tethys, Egypt: Insights from the mineralogy and geochemistry of Upper Cretaceous lacustrine organic-rich deposits. *Cretac. Res.* **2021**, *126*, 104880. [[CrossRef](#)]
9. Zhu, X.; Chen, J.; Li, W.; Pei, L.; Liu, K.; Chen, X.; Zhang, T. Hydrocarbon generation potential of Paleogene coals and organically rich mudstones in Xihu sag, East China Sea Shelf basin, offshore eastern China. *J. Pet. Sci. Eng.* **2020**, *184*, 106450. [[CrossRef](#)]
10. Tao, S.-Z.; Zou, C.-N. Accumulation and distribution of natural gases in Xihu Sag, East China Sea Basin. *Pet. Explor. Dev.* **2005**, *32*, 103–110.
11. Zhu, Y.; Li, Y.; Zhou, J.; Gu, S. Geochemical characteristics of Tertiary coal-bearing source rocks in Xihu depression, East China Sea basin. *Mar. Pet. Geol.* **2012**, *35*, 154–165. [[CrossRef](#)]
12. Cheng, X.; Hou, D.; Zhao, Z.; Chen, X.; Diao, H. Sources of Natural Gases in the Xihu Sag, East China Sea Basin: Insights from Stable Carbon Isotopes and Confined System Pyrolysis. *Energy Fuels* **2019**, *33*, 2166–2175. [[CrossRef](#)]
13. Xu, H.; George, S.C.; Hou, D.; Cao, B.; Chen, X. Petroleum sources in the Xihu Depression, East China Sea: Evidence from stable carbon isotopic compositions of individual n-alkanes and isoprenoids. *J. Pet. Sci. Eng.* **2020**, *190*, 107073. [[CrossRef](#)]
14. Fu, N. Diterpenoid compounds in coal measures and condensates in Xihu Sag of East China Sea Basin. *China Offshore Oil Gas* **1994**, *8*, 21–28.
15. Cheng, X.; Hou, D.; Zhou, X.; Liu, J.; Diao, H.; Jiang, Y.; Yu, Z. Organic geochemistry and kinetics for natural gas generation from mudstone and coal in the Xihu Sag, East China Sea Shelf Basin, China. *Mar. Pet. Geol.* **2020**, *118*, 104405. [[CrossRef](#)]
16. Kang, S.; Shao, L.; Qin, L.; Li, S.; Liu, J.; Shen, W.; Chen, X.; Eriksson, K.A.; Zhou, Q. Hydrocarbon Generation Potential and Depositional Setting of Eocene Oil-Prone Coaly Source Rocks in the Xihu Sag, East China Sea Shelf Basin. *ACS Omega* **2020**, *5*, 32267–32285. [[CrossRef](#)]
17. Cheng, X.; Hou, D.J.; Zhao, Z.; Jiang, Y.H.; Zhou, X.H.; Diao, H. Higher Landplant -Derived Biomarkers in Light Oils and Condensates from the Coal-Bearing Eocene Pinghu Formation, Xihu Sag, East China Sea Shelf Basin. *J. Pet. Geol.* **2020**, *43*, 437–451. [[CrossRef](#)]
18. Weilin, Z.; Kai, Z.; Xiaowei, F.; Chunfeng, C.; Minqiang, Z.; Shunli, G. The formation and evolution of the East China Sea Shelf Basin: A new view. *Earth-Sci. Rev.* **2019**, *190*, 89–111. [[CrossRef](#)]
19. Zhou, Z.W.; Zhao, J.H.; Yin, P.L. *Characteristics and Tectonic Evolution of the East China Sea*; Elsevier: Oxford, UK, 1989.
20. Abbas, A.; Zhu, H.; Zeng, Z.; Zhou, X. Sedimentary facies analysis using sequence stratigraphy and seismic sedimentology in the Paleogene Pinghu Formation, Xihu Depression, East China Sea Shelf Basin. *Mar. Pet. Geol.* **2018**, *93*, 287–297. [[CrossRef](#)]
21. Yu, S. Depositional genesis analysis of source rock in Pinghu Formation of Western Slope, Xihu Depression. *Earth Sci.* **2020**, *45*, 1722–1736.
22. Wang, Y.; Qin, Y.; Yang, L.; Liu, S.; Elsworth, D.; Zhang, R. Organic Geochemical and Petrographic Characteristics of the Coal Measure Source Rocks of Pinghu Formation in the Xihu Sag of the East China Sea Shelf Basin: Implications for Coal Measure Gas Potential. *Acta Geol. Sin. -Engl. Ed.* **2020**, *94*, 364–375. [[CrossRef](#)]
23. Liu, J.; Kang, S.; Shen, W.; Qin, L.; Zhou, Q.; Li, S.; Ding, F.; Shao, L. Petrology and hydrocarbon significance of the coaly source rocks from the Pinghu Formation in the Xihu Sag, East China Sea Shelf Basin. *Energy Explor. Exploit.* **2020**, *38*, 1295–1319. [[CrossRef](#)]
24. Jiang, Y.; Diao, H.; Zeng, W. Coal source rock conditions and hydrocarbon generation model of Pinghu Formation in Xihu Depression, East China Sea Basin. *Bull. Geol. Sci. Technol.* **2020**, *39*, 30–39.
25. Peters, K.E.; Cassa, M.R.; Magoon, L.B.; Dow, W.G. Applied Source Rock Geochemistry. In *The Petroleum System—From Source to Trap*; American Association of Petroleum Geologists: Tulsa, OK, USA, 1994; Volume 60, pp. 93–120.
26. Cheng, X.; Hou, D.; Xu, C.; Wang, F. Biodegradation of tricyclic terpanes in crude oils from the Bohai Bay Basin. *Org. Geochem.* **2016**, *101*, 11–21. [[CrossRef](#)]
27. Barrick, R.C.; Hedges, J.I. Hydrocarbon geochemistry of the Puget Sound region—II. Sedimentary diterpenoid, steroid and triterpenoid hydrocarbons. *Geochim. Et Cosmochim. Acta* **1981**, *45*, 381–392. [[CrossRef](#)]
28. Noble, R.A.; Alexander, R.; Kagi, R.I.; Knox, J. Tetracyclic diterpenoid hydrocarbons in some Australian coals, sediments and crude oils. *Geochim. Et Cosmochim. Acta* **1985**, *49*, 2141–2147. [[CrossRef](#)]
29. Bray, E.E.; Evans, E.D. Distribution of n-paraffins as a clue to recognition of source beds. *Geochim. Et Cosmochim. Acta* **1961**, *22*, 2–15. [[CrossRef](#)]
30. Bourbonniere, R.A.; Meyers, P.A. Sedimentary geolipid records of historical changes in the watersheds and productivities of Lakes Ontario and Erie. *Limnol. Oceanogr.* **1996**, *41*, 352–359. [[CrossRef](#)]
31. Ficken, K.J.; Li, B.; Swain, D.L.; Eglinton, G. An n-alkane proxy for the sedimentary input of submerged/floating freshwater aquatic macrophytes. *Org. Geochem.* **2000**, *31*, 745–749. [[CrossRef](#)]
32. Zheng, Y.; Zhou, W.; Meyers, P.A.; Xie, S. Lipid biomarkers in the Zoigê-Hongyuan peat deposit: Indicators of Holocene climate changes in West China. *Org. Geochem.* **2007**, *38*, 1927–1940. [[CrossRef](#)]
33. Bechtel, A.; Sachsenhofer, R.F.; Kolcon, I.; Gratzner, R.; Otto, A.; Püttmann, W. Organic geochemistry of the Lower Miocene Oberdorf lignite (Styrian Basin, Austria): Its relation to petrography, palynology and the palaeoenvironment. *Int. J. Coal Geol.* **2002**, *51*, 31–57. [[CrossRef](#)]
34. Seifert, W.K.; Moldowan, J.M. The effect of thermal stress on source-rock quality as measured by hopane stereochemistry. *Phys. Chem. Earth* **1980**, *12*, 229–237. [[CrossRef](#)]
35. Cranwell, P.A. Organic geochemistry of Cam Loch (Sutherland) sediments. *Chem. Geol.* **1977**, *20*, 205–221. [[CrossRef](#)]

36. Eglinton, G.; Hamilton, R.J. Leaf epicuticular waxes. *Science* **1967**, *156*, 1322–1335. [[CrossRef](#)] [[PubMed](#)]
37. Gelpi, E.; Schneider, H.; Mann, J.; Oró, J. Hydrocarbons of geochemical significance in microscopic algae. *Phytochemistry* **1970**, *9*, 603–612. [[CrossRef](#)]
38. Philp, R. Geochemical characteristics of oils derived predominantly from terrigenous source materials. *Geol. Soc. Lond. Spec. Publ.* **1994**, *77*, 71–91. [[CrossRef](#)]
39. Huang, W.-Y.; Meinschein, W.G. Sterols as ecological indicators. *Geochim. Et Cosmochim. Acta* **1979**, *43*, 739–745. [[CrossRef](#)]
40. Volkman, J.K. A review of sterol markers for marine and terrigenous organic matter. *Org. Geochem.* **1986**, *9*, 83–99. [[CrossRef](#)]
41. Ourisson, G.; Albrecht, P.; Rohmer, M. The Hopanoids: Palaeochemistry and biochemistry of a group of natural products. *Pure Appl. Chem.* **1979**, *51*, 709–729. [[CrossRef](#)]
42. Alexander, R.; Kagi, R.I.; Noble, R.; Volkman, J.K. Identification of some bicyclic alkanes in petroleum. *Org. Geochem.* **1984**, *6*, 63–72. [[CrossRef](#)]
43. Philp, R.P. *Fossil Fuel Biomarkers. Methods in Geochemistry and Geophysics*; Elsevier: Amsterdam, The Netherlands, 1981.
44. Otto, A.; Wilde, V. Sesqui-, Di-, and triterpenoids as chemosystematic markers in extant conifers—A review. *Bot. Rev.* **2001**, *67*, 141–238. [[CrossRef](#)]
45. Dimmler, A.; Cyr, T.D.; Strausz, O.P. Identification of bicyclic terpenoid hydrocarbons in the saturate fraction of Athabasca oil sand bitumen. *Org. Geochem.* **1984**, *7*, 231–238. [[CrossRef](#)]
46. Otto, A.; Simoneit, B.R.T. Biomarkers of Holocene buried conifer logs from Bella Coola and north Vancouver, British Columbia, Canada. *Org. Geochem.* **2002**, *33*, 1241–1251. [[CrossRef](#)]
47. Diefendorf, A.F.; Leslie, A.B.; Wing, S.L. A phylogenetic analysis of conifer diterpenoids and their carbon isotopes for chemotaxonomic applications. *Org. Geochem.* **2019**, *127*, 50–58. [[CrossRef](#)]
48. Noble, R.A.; Alexander, R.; Kagi, R.I.; Nox, J.K. Identification of some diterpenoid hydrocarbons in petroleum. *Org. Geochem.* **1986**, *10*, 825–829. [[CrossRef](#)]
49. Weston, R.J.; Philp, R.P.; Sheppard, C.M.; Woolhouse, A.D. Sesquiterpanes, diterpanes and other higher terpanes in oils from the Taranaki basin of New Zealand. *Org. Geochem.* **1989**, *14*, 405–421. [[CrossRef](#)]
50. Simoneit, B. Cyclic terpenoids of the geosphere. *Methods Geochem. Geophys.* **1986**, *24*, 43–99.
51. Killops, S.D.; Raine, J.I.; Woolhouse, A.D.; Weston, R.J. Chemostratigraphic evidence of higher-plant evolution in the Taranaki Basin, New Zealand. *Org. Geochem.* **1995**, *23*, 429–445. [[CrossRef](#)]
52. Trendel, J.M.; Lohmann, F.; Kintzinger, J.P.; Albrecht, P.; Chiarone, A.; Riche, C.; Cesario, M.; Guilhem, J.; Pascard, C. Identification of des-A-triterpenoid hydrocarbons occurring in surface sediments. *Tetrahedron* **1989**, *45*, 4457–4470. [[CrossRef](#)]
53. Otto, A.; Walther, H.; Puttmann, W. Sesqui- and diterpenoid biomarkers preserved in Taxodium-rich Oligocene oxbow lake clays, Weissenster basin, Germany. *Org. Geochem.* **1997**, *26*, 105–115. [[CrossRef](#)]
54. Regnery, J.; Puttmann, W.; Koutsodendris, A.; Mulch, A.; Pross, J. Comparison of the paleoclimatic significance of higher land plant biomarker concentrations and pollen data: A case study of lake sediments from the Holsteinian interglacial. *Org. Geochem.* **2013**, *61*, 73–84. [[CrossRef](#)]
55. Didyk, B.; Simoneit, B.; Brassell, S.; Eglinton, G. Organic geochemical indicators of paleoenvironmental conditions of sedimentation. *Nature* **1978**, *272*, 216–222. [[CrossRef](#)]
56. Goossens, H.; de Leeuw, J.; Schenck, P.A.; Brassell, S. Tocopherols as likely precursors of pristane in ancient sediments and crude oils. *Nature* **1984**, *312*, 440–442. [[CrossRef](#)]
57. Koopmans, M.P.; Rijpstra, W.I.C.; Klapwijk, M.M.; de Leeuw, J.W.; Lewan, M.D.; Sinninghe Damsté, J.S. A thermal and chemical degradation approach to decipher pristane and phytane precursors in sedimentary organic matter. *Org. Geochem.* **1999**, *30*, 1089–1104. [[CrossRef](#)]
58. Peters, K.E.; Walters, C.C.; Moldowan, J.M. *The Biomarker Guide: Volume 2: Biomarkers and Isotopes in Petroleum Systems and Earth History*, 2nd ed.; Cambridge University Press: Cambridge, UK, 2004; Volume 2.
59. Rubinstein, I.; Sieskind, O.; Albrecht, P. Rearranged sterenes in a shale: Occurrence and simulated formation. *J. Chem. Soc. Perkin Trans.* **1975**, *1*, 1833–1836. [[CrossRef](#)]
60. Moldowan, J.M.; Sundararaman, P.; Schoell, M. Sensitivity of biomarker properties to depositional environment and/or source input in the Lower Toarcian of SW-Germany. *Org. Geochem.* **1986**, *10*, 915–926. [[CrossRef](#)]
61. Seifert, W.K.; Michael Moldowan, J. Applications of steranes, terpanes and monoaromatics to the maturation, migration and source of crude oils. *Geochim. Et Cosmochim. Acta* **1978**, *42*, 77–95. [[CrossRef](#)]
62. Wan Hasiah, A. Oil-generating potential of Tertiary coals and other organic-rich sediments of the Nyalau Formation, onshore Sarawak. *J. Asian Earth Sci.* **1999**, *17*, 255–267. [[CrossRef](#)]
63. Mackenzie, A.S.; Patience, R.L.; Maxwell, J.R.; Vandenbroucke, M.; Durand, B. Molecular parameters of maturation in the Toarcian shales, Paris Basin, France—I. Changes in the configurations of acyclic isoprenoid alkanes, steranes and triterpanes. *Geochim. Et Cosmochim. Acta* **1980**, *44*, 1709–1721. [[CrossRef](#)]
64. Seifert, W.; Moldowan, J. Use of biological markers in petroleum exploration. *Methods Geochem. Geophys.* **1986**, *24*, 261–290.
65. Wilkins, R.W.T.; George, S.C. Coal as a source rock for oil: A review. *Int. J. Coal Geol.* **2002**, *50*, 317–361. [[CrossRef](#)]
66. Snowdon, L.R. Oil from Type III organic matter: Resinite revisited. *Org. Geochem.* **1991**, *17*, 743–747. [[CrossRef](#)]
67. Hunt, J.M. Generation of gas and oil from coal and other terrestrial organic matter. *Org. Geochem.* **1991**, *17*, 673–680. [[CrossRef](#)]

- 
68. Tissot, B.; Durand, B.; Espitalie, J.; Combaz, A. Influence of Nature and Diagenesis of Organic Matter in Formation of Petroleum. *AAPG Bull.* **1974**, *58*, 499–506.
  69. Sykes, R.; Snowdon, L.R. Guidelines for assessing the petroleum potential of coaly source rocks using Rock-Eval pyrolysis. *Org. Geochem.* **2002**, *33*, 1441–1455. [[CrossRef](#)]